Determining finite-width-correction factors for fatigue crack growth prediction in GLARE using the equivalent compliance method

Zhao, Yuan; Alderliesten, René; Wu, Zengwen; Zhou, Zhengong; Fang, Guodong; Zhang, Jiazhen; Benedictus, Rinze

DOI
10.1016/j.ijfatigue.2019.05.037

Publication date
2019

Document Version
Final published version

Published in
International Journal of Fatigue

Citation (APA)
Zhao, Y., Alderliesten, R., Wu, Z., Zhou, Z., Fang, G., Zhang, J., & Benedictus, R. (2019). Determining finite-width-correction factors for fatigue crack growth prediction in GLARE using the equivalent compliance method. *International Journal of Fatigue*, *127*, 74-81. https://doi.org/10.1016/j.ijfatigue.2019.05.037

International Journal of Fatigue 127 (2019) 74–81

Contents lists available at ScienceDirect

International Journal of Fatigue

journal homepage: www.elsevier.com/locate/ijfatigue

Determining finite-width-correction factors for fatigue crack growth prediction in GLARE using the equivalent compliance method

Yuan Zhao[a,b], René Alderliesten[b], Zengwen Wu[a], Zhengong Zhou[a], Guodong Fang[a,*], Jiazhen Zhang[a], Rinze Benedictus[b]

[a] Science and Technology on Advanced Composites in Special Environments Key Laboratory, Harbin Institute of Technology, Harbin 150001, PR China
[b] Structural Integrity & Composites Group, Faculty of Aerospace Engineering, Delft University of Technology, Kluyverweg 1, 2629 HS Delft, the Netherlands

ARTICLE INFO

Keywords:
Finite-width-correction factor
GLARE
Compliance
Applied work
Delamination

ABSTRACT

Finite-width-correction factors (FWCF) are required for GLARE to accurately predict fatigue crack growth using linear elastic fracture mechanics. As demonstrated in earlier work, these factors effectively correct for the change in specimen compliance, which in GLARE relates to intact fibre layers and the formation of delaminations between these layers and the cracked metal layers. Therefore, the development of delaminations in various GLARE grades were studied using digital image correlation during fatigue crack growth experiments under different maximum stresses and stress ratios. The elongation of GLARE in loading direction was recorded by crosshead displacement during fatigue testing, and was correlated to the observed development of the delamination area. The relationship between effective delamination area and effective GLARE specimen compliance is used as basis for determining explicit formulations for the FWCF for GLARE.

1. Introduction

GLARE is a fibre metal laminate (FML) with inherently higher fatigue crack growth resistance, high impact resistance, damage tolerance, and high burn through resistance than monolithic aluminium. It has been applied in the primary fuselage structure of the Airbus A380. The current understanding of fatigue crack propagation in FMLs is formulated using linear elastic fracture mechanics, in which an effective stress intensity factor (SIF) is calculated by using the principle of superposition, and subsequently applied in a Paris-type relation to calculate the crack growth rate [1,2]. The superposition includes the SIF of a centre crack in a monolithic plate under far field uniaxial loading and the SIF for the bridging stresses of fibres restraining the crack opening [3]. Some corrections then should be applied to calculate the SIF of FMLs under fatigue loading, including a Finite-Width-Correction Factor (FWCF), a stress ratio correction, and a delamination correction [4]. However, Alderliesten [5] and Wilson [6] observed that the traditional FWCF for centre cracks in a monolithic plate was not suitable for FMLs, as it would result in over-predicting the fatigue crack growth. Nonetheless, theoretically one can expect that a FWCF for FMLs should be incorporated in the calculation of the effective SIF. The SIF for any finite geometry needs correction factors, which are stipulated by the many studies on development of weigth functions.

In the past, several researchers have studied the FWCF to establish a relationship between the crack tip SIF for uniformly stressed strip with a through-thickness centre crack and the closed form solutions of SIF for infinite width plate. Westergaard [7] and Koiter [8] obtained a relation for the FWCF by correlating the stress field equation for finite width strip and the linear elastic tress field equations for infinite width plate. Irwin [9] suggested an approximate formula for the crack tip SIF by solving a periodic array of cracks in an infinite sheet under uniform stress. Isida [10] obtained the SIF correction by using series expansion stress function techniques. Other approximate polynomial forms for FWCF for central crack problems were developed by Brown and Srawley [11], Forman and Kobayashi [11,12] and Tada [13]. Feddersen [14] provided a concise secant formula for SIF correction very close to the approximate polynomial forms. Dixon [15] developed a theoretical solution of FWCF for centre cracked plates, which was verified by photoelastic experiments. It should be noted that discrepancies exist in the above corrections when the aspect ratio of crack length and plate width is close to 1. Bowie and Neal [16] used a modified mapping collocation technique to illustrate this phenomenon. As for the nonlinear effect, such as crack front plastic yielding, Irwin used a plastic zone size correction as a means to compensate [17]. Liebowifz and Eftis [18] adopted total strain energy dissipation rate using a simple compliance type determination to study the nonlinear effect. The

* Corresponding author.
E-mail address: fanggd@hit.edu.cn (G. Fang).

https://doi.org/10.1016/j.ijfatigue.2019.05.037
Received 1 February 2019; Received in revised form 30 May 2019; Accepted 31 May 2019
Available online 01 June 2019
0142-1123/

Nomenclature

Symbol	Description [Unit]
a	half crack length [mm]
a_0	half starter crack length [mm]
a_{max}	theoretical maximum crack length [mm]
A	delamination area [mm^2]
$A_{\max}$	theoretical maximum delamination area [mm^2]
b	half delamination length [mm]
b_{eq}	equivalent half delamination lengh across the specimen width [mm]
E_{FML}	Young's modulus of the entire laminate [MPa]
E_f	Young's modulus of all fibre layers together [GPa]
E_{f0}	longitudinal Young's modulus of fibre layers [MPa]
E_{f90}	transverse Young's modulus of fibre layers [MPa]
L	specimen length [mm]
ΔL	specimen elongation [mm]
n_{Al}	number of aluminium layers [-]
n_{f0}	number of fibre layers parallel to the loading direction [-]
n_{f90}	number of fibre layers perpendicular to the loading direction [-]
P	load [N]
t_{Al}	thickness of aluminium layer [mm]
t_f	thickness of fibre layer [mm]
t_{FML}	thickness of entire laminate [mm]
W	specimen width [mm]
λ_{eq}	equivalent compliance [-]
λ_{FML}	compliance of the laminate [-]
λ_f	compliance of all fibre layers [-]
F_0	FWCF for monolithic metal material [-]
$F(a)$	finite-width-correction factor [-]
F_f	finite-width-correction factor from delamination [-]

relationship between the strain energy dissipation rate and SIF is obtained when a specimen has a small crack increment without changing its length. This is often referred to as 'fixed grip condition'. Chandran [19] related the FWCF to the average net-section stress using an imaginary of cutting and welding a finite width specimen in an infinite plate.

In the current work, we extend the hypothesis discussed in [20], i.e. the FWCF is related to the change in applied work under constant amplitude loading, with the hypothesis that this change in compliance in GLARE relates to the actual delamination size. Therefore, the delamination areas for different GLARE grades under fatigue loading were measured to calculate the change in specimen compliances. It is hypothesized that a relationship between the specimen compliance and the delamination size, enables to find an explicit formulation for the FWCF for any GLARE grade of which the delamination sizes is predicted. Therefore, this paper presents the experiments, the measurement of delamination growth during the tests, and presents an explicit relationship for the FWCF through correlation with specimen compliance.

2. Experiment

To evaluate the fatigue crack growth behavior and delamination characteristics of GLARE under fatigue loading, fatigue experiments with different maximum applied stresses and stress ratios of GLARE with different grades were conducted. The test matrix is provided in Table 1. The basic mechanical properties of Aluminium 2024-T3 and Prepreg S2/FM94 are presented in Table 2 [21]. There are three standard grades of GLARE used in the test: GLARE 2A-4/3-0.4, GLARE3-5/4-0.4 and GLARE4B-5/4-04. GLARE 2A, GLARE3 and GLARE4B are, respectively, corresponding to 0/0, 0/90 and 90/0/90 of fibre layer orientations with respect to the rolling direction of the aluminium. The '4/3' in GLARE 2A-4/3-0.4 represents the alternative distribution for 4 layers of 2024-T3 aluminium and 3 layers of 0/0 fibre prepreg, while 0.4 in GLARE 2A-4/3-0.4 indicates a thickness of 0.4 mm for each 2024-T3 aluminium layer. As for each grade of GLARE, three levels of maximum applied stresses and two stress ratios were applied. The geometry and dimensions of the fatigue specimen are derived from the ASTM E647-15el standard [22], as illustrated in Fig. 1(a). A hole with a radius of 1.5 mm was drilled in the centre of the specimen. Two opposite initial saw-cuts of length 1 mm were made at the hole edges, to create a starter crack of $2a_0 = 5$ mm. This precrack condition might not be representative for a crack initiating at a rivet hole in one of the metal layers of an FML, because not all layers are initially cut (including fibre layers), but just a single layer. However, the motivation for choosing this through-thickness crack geometry in Fig. 1 originates in the lower level of complexity, allowing better understanding of the fatiguie crack growth phenomena. Most studies adopted this through-thickness crack configuration, which allows the current work to be related to previous studies. Additionally, the centre crack configuration is preferred over e.g. compact tension, because the centre crack opening of the crack is more realistic and representative for actual cracks in structures. Compact tension gives too much rotation opening of the crack, which in practice does not occur.

Fig. 1(b) shows the measurement setup. All fatigue tests were conducted with constant amplitude load spectrum on an MTS 250 kN fatigue testing machine. The fatigue loading frequency was 10 Hz. Speckle patterns were sprayed on all specimens to record fatigue crack lengths and subsurface delamination shapes during the fatigue tests through digital image correlation (DIC). The method to measure and obtain crack length and delamination from DIC has already been introduced in earlier studies, like Khan and Rodi [23,24]. The delamination shapes and sizes obtained by DIC are well consistent with the ones obtained by chemical etching [24,25]. In addition, the crosshead displacements were recorded, which were observed to increase during the constant amplitude fatigue load due to the increase of compliance of the GLARE specimens. It should be noted that these crosshead displacements include errors from fixture and crossbeam.

3. Compliance calculation using equivalent delamination area

The change in compliance can be calculated with the change in specimen stiffness. Traditionally, this apparent stiffness change is related to the crack length. In GLARE, this should be related to both the formation of cracks and of delaminations. Hence, instead of simply determining compliance through crosshead displacement and force and relating it to crack length over width, one should relate compliance to crack length over width and delamination area over the specimen's aerial dimensions. Fig. 2 shows the DIC strains illustrating the delamination contours of GLARE 3 under fatigue loading corresponding to

Table 1
Test matrix for fatigue experiments of GLARE.

Material	Maximum Stress [MPa]	Stress Ratio [-]	Specimen name
GLARE 2A-4/3-0.4	160	0.05	G2AS160R0.05
	200	0.05	G2AS200R0.05
	240	0.5	G2AS240R0.5
GLARE 3-5/4-0.4	120	0.05	G3S120R0.05
	180	0.5	G3S180R0.5
	200	0.5	G3S200R0.5
GLARE 4B-5/4-0.4	100	0.05	G4BS100R0.05
	120	0.05	G4BS120R0.05
	180	0.5	G4BS180R0.5

Table 2
Mechanical properties of Aluminium 2024-T3 and Pregreg S2/FM94 [21]

	Unit	2024-T3	S2-glass, FM-94	
			‖Fibre axis	⊥Fibre axis
Thickness of single layer	mm	0.4	0.133	
Young's Modulus	MPa	72,400	48,900	5500
Shear Modulus	MPa	27,600	5550	
Poisson's ratio υ_{xy}	–	0.33		
Poisson's ratio υ_{yx}	–	0.33	0.0371	
Thermal expansion coefficient	$10^{-6}°C^{-1}$	22	6.1	26.2
Curing temperature	°C	–	120	

different fatigue crack lengths. The subsurface delamination shapes in Fig. 2 between fibre layer and aluminum layer can be distinguished through the difference of strains in the delaminated and non-delaminated regions. Thus, the delamination contours for each GLARE specimen were recorded during the fatigue tests using non-destructive DIC.

The schematic diagram of delamination contour is shown in Fig. 1, where a is the fatigue crack length, and b is the maximum width of delamination region along the loading direction. In the delaminated region, the metal layers do not carry load owing to the existence of fatigue crack, implying that all load in the aluminum layers is transfered to the fibre layers. The fibre layers carry the load, because they are not broken at the location where the metal is cracked [23]. The delamination areas can be quantified by integrating each delamination shape corresponding to each fatigue crack length. Fig. 3 shows a series of one quarter delamination contours, which were used to calculate the delamination area by using finite element discretization. It can be found that the delamination shapes corresponding to different crack lengths are different. The delamination area is related with the energy dissipation.

In order to calculate the compliance of GLARE specimen, an equivalent rectangular area is assumed, which is described by the specimen width W and a delamination length $2b_{eq}$. Thus, the area defined by $2b_{eq}W$ is equal to the delamination area of the real delamination contour as shown in Fig. 1. Theoretically, the fatigue specimen then can be divided into two non-delaminated regions and a delaminated region defined by $2b_{eq}W$, as shown in Fig. 1. By a linear simplication of the Classical Laminate Theory, the stiffness of the specimen in the non-delaminated region can be calculated as

$$E_{FML} = \frac{E_{al}\cdot n_{al}\cdot t_{al} + E_{f0}\cdot n_{f0}\cdot t_f + E_{f90}\cdot n_{f90}\cdot t_f}{n_{al}\cdot t_{al} + n_{f0}\cdot t_f + n_{f90}\cdot t_f} \tag{1}$$

In the delaminated region, only the fibre layers carry the fatigue load. Thus, the stiffness of the specimen in the region can be expressed as

$$E_f = \frac{E_{f0}\cdot n_{f0}\cdot t_f + E_{f90}\cdot n_{f90}\cdot t_f}{n_{f0}\cdot t_f + n_{f90}\cdot t_f} \tag{2}$$

Along the fatigue loading direction, the equivalent compliance of GLARE can be calculated using the compliances of non-delaminated

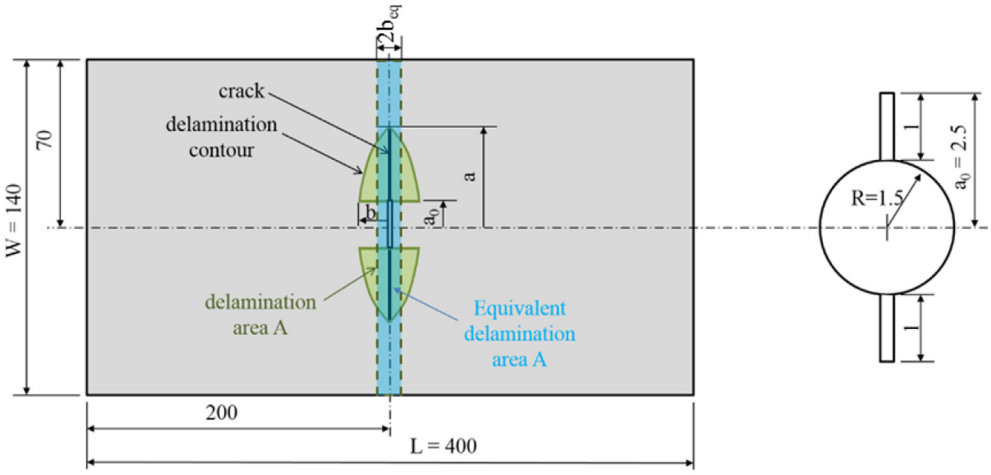

(a)

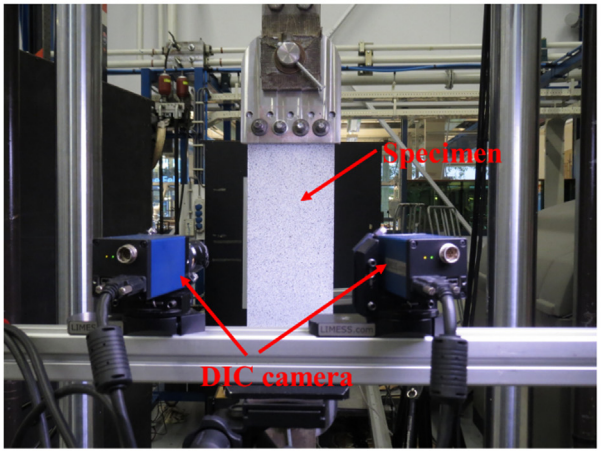

(b)

Fig. 1. (a) Geometry sizes of fatigue specimen (all dimensions in mm) for GLARE and (b) measurement setup.

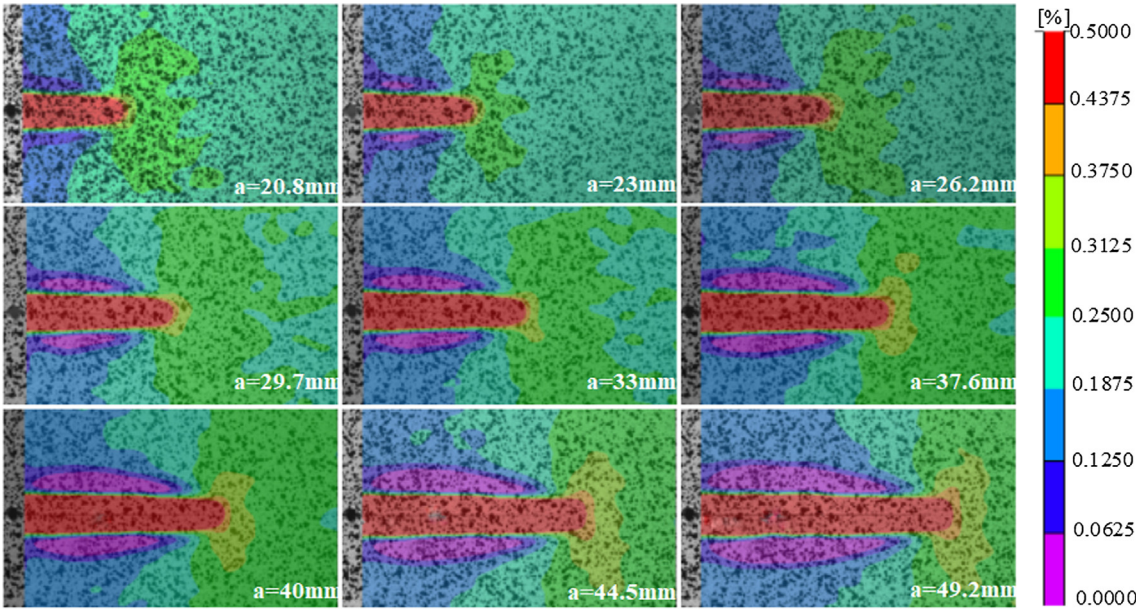

Fig. 2. DIC E_{yy} strains illustrating delamination contours of GLARE 3 corresponding to different fatigue crack lengths.

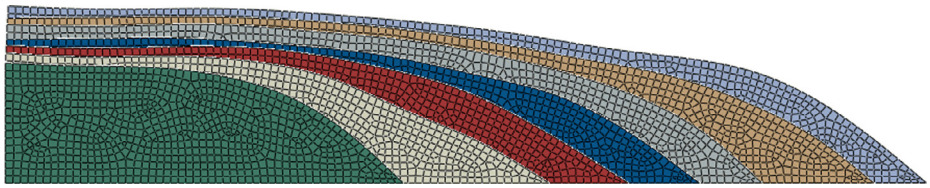

Fig. 3. A series of delamination contours.

and delaminated regions, expressed as

$$\lambda eq \cdot P \cdot L = \lambda_{FML} \cdot P \cdot (L - 2b_{eq}) + \lambda_f \cdot P \cdot 2b_{eq}$$
$$\lambda_{eq} \cdot P \cdot L = \lambda FML \cdot P \cdot (L - 2b_{eq}) + \lambda f \cdot P \cdot 2b_{eq} \quad (3)$$

where $2b_{eq}$ is the equivalent delamination length along the loading direction, as shown in Fig. 1. The compliance ratios of non-delaminated and delaminated regions are

$$\lambda_{FML} = \frac{1}{E_{FML} \cdot W \cdot (n_{Al} \cdot t_{Al} + n_{f0} t_f + n_{f90} t_f)} \quad (4)$$

$$\lambda_f = \frac{1}{E_f \cdot W \cdot (n_{f0} t_f + n_{f90} t_f)} \quad (5)$$

The elongation of the specimen during the fatigue experiment as a result of the change in compliance can be written as

$$\Delta L = P \cdot (\lambda_{eq} - \lambda_{FML}) \quad (6)$$

which is used to calculate the elongation of the specimen during the fatigue experiment, and is necessary to quantify the change in applied work (strain energy). Here, the FWCF is the ratio of the applied work U_N and original applied work U_0, which can be expressed as

$$F(a) = \frac{U_N}{U_0} = \frac{0.5P^2\lambda_{eq}}{0.5P^2\lambda_{FML}} = \frac{\lambda_{eq}}{\lambda_{FML}} \quad (7)$$

Theoretically, the FWCF can be divided into two parts:

$$F(a) = F_0\left(\frac{2a}{W}\right) F_f\left(\frac{A}{A_{\max}}\right) \quad (8)$$

where $F_0(2a/W)$ is the common FWCF for monolithic metal material, for which in the present study the Dixon FWCF is taken, i.e. $F_0\left(\frac{2a}{W}\right) = 1/\sqrt{1 - \left(\frac{2a}{W}\right)^2}$. $F_f\left(\frac{A}{A_{\max}}\right)$ is then the correction for the delamination in GLARE, and $A_{\max}$ is the maximum delamination area corresponding to the maximum crack $a_{\max} = W/2$.

4. Results and discussions

4.1. Delamination area and compliance of GLARE under fatigue loading

The subsurface delamination shapes corresponding to different fatigue crack lengths can be measured using DIC measurements. Takamatsu et al. has studied the differences between interior subsurface cracks and surface cracks in GLARE, and reported differences of few %, i.e. marginally shorter cracks and delamination lengths at inner layers [27]. This difference is ignored in the present study. Therefore, it is assumed here that the delamination areas in the interior of GLARE are the same as the one subsurface measured through DIC, shown in Fig. 2. The equations fitting the delamination area measured with DIC to $2a/W$ are listed in the Table 3. The fitting curves and the experimental data for GLARE 2A, GLARE 3 and GLARE 4B are provided in Fig. 4.

Fig. 4 illustrates that the fatigue delamination growth in all specimens is related to the maximum stress and the stress ratio. For example,

Table 3
Fitting curves of delamination area and $2a/W$ for different kinds of GLARE.

Serial No.	Smax (MPa)	R	Fitting Equation of Quarter Delamination Area
G2AS160R0.05	160	0.05	$A = 884.09 \times (2a/W)^{1.76}$
G2AS200R0.05	200	0.05	$A = 1004.4 \times (2a/W)^{1.84}$
G2AS240R0.5	240	0.5	$A = 698.74 \times (2a/W)^{1.75}$
G3S120R0.05	120	0.05	$A = 698.66 \times (2a/W)^{1.63}$
G3S180R0.5	180	0.5	$A = 675.07 \times (2a/W)^{1.81}$
G3S200R0.5	200	0.5	$A = 922.7 \times (2a/W)^{2.12}$
G4BS100R0.05	100	0.05	$A = 660.68 \times (2a/W)^{1.67}$
G4BS120R0.05	120	0.05	$A = 719.19 \times (2a/W)^{1.64}$
G4BS180R0.5	180	0.5	$A = 817.41 \times (2a/W)^{2.05}$

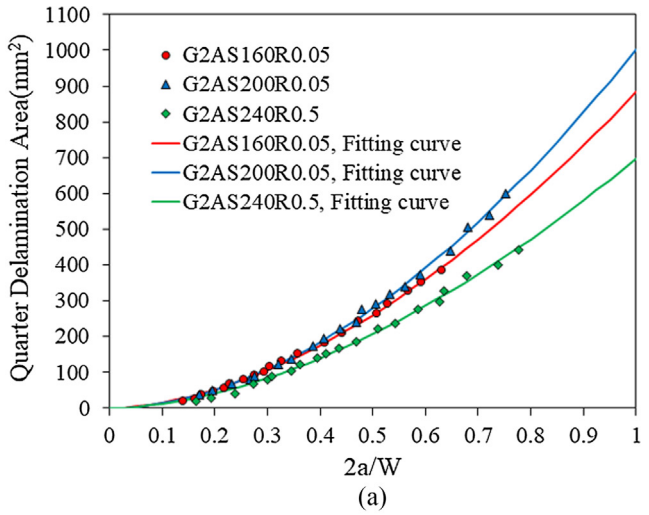

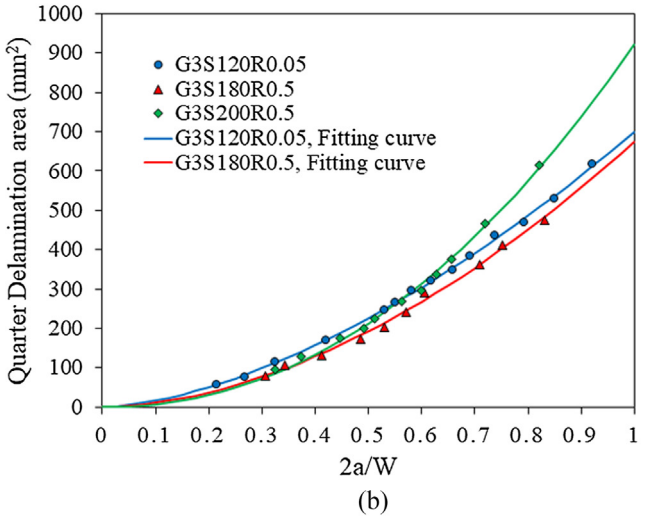

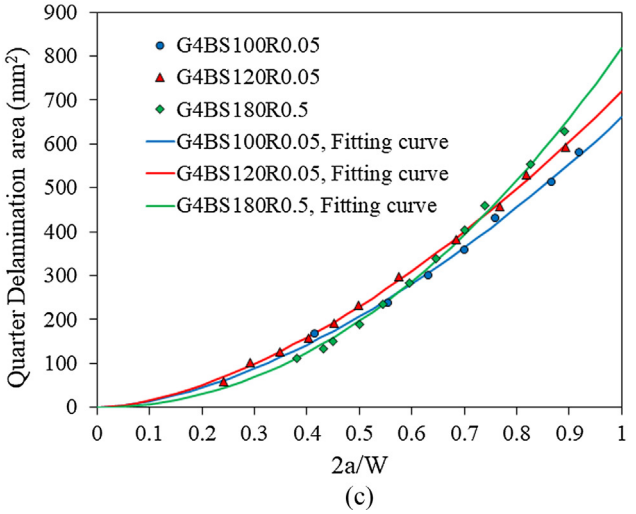

Fig. 4. Delamination area against $2a/W$ curves, (a) GLARE 2A, (b) GLARE 3, and (c) GLARE 4B.

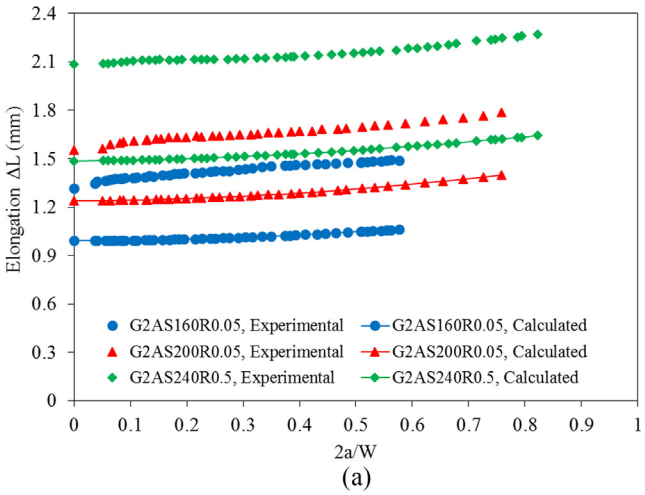

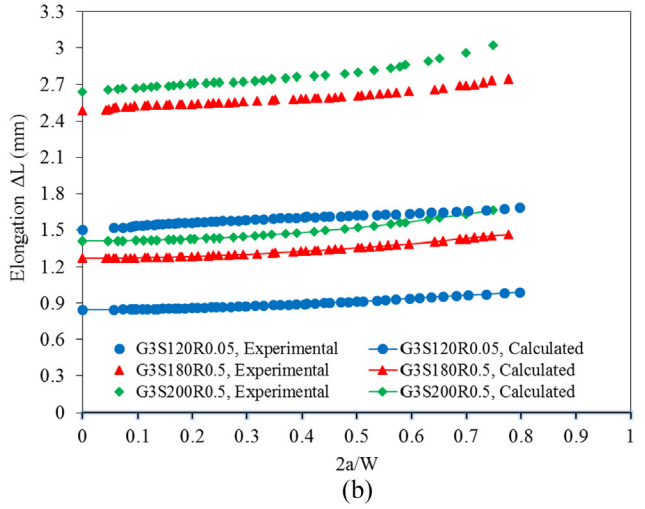

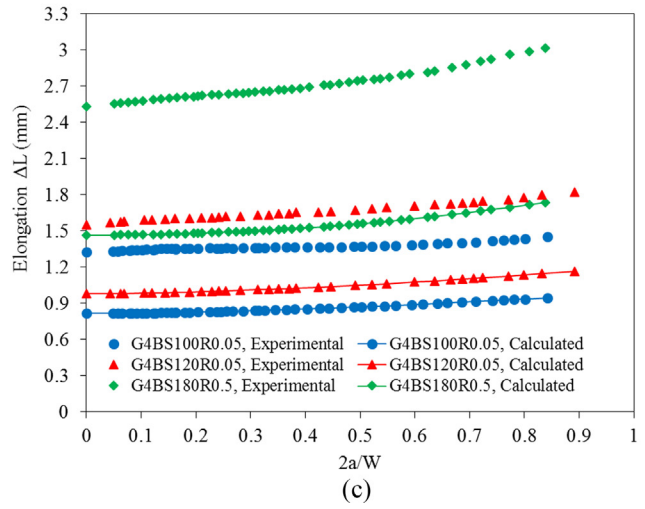

Fig. 5. Elongation calculated by equivalent delamination area and comparing with the crosshead displacement measured in the experiment, (a) GLARE 2A, (b) GLARE 3, and (c) GLARE 4B.

the delamination growth at a stress ratio of R = 0.05 is higher than that at a stress ratio of R = 0.5. Similarly, a larger maximum stress corresponds to a larger delamination area at the same stress ratio. Additionally, the maximum delamination area for each specimen can be determined theoretically by extrapolating the fitting equation in Table 3 to the crack length $a = W/2$.

The specimen elongations during fatigue testing were recorded through the crosshead displacement. These elongations are compared to the elongations calculated with the equivalent delaminations for GLARE 2A, GLARE 3 and GLARE 4B in Fig. 5. This figure illustrates that the calculated elongation of each specimen along the loading direction is smaller than the crosshead displacement, while the trend is similar.

This is attributed to the fact that the crosshead displacement includes not only the specimen deformation but also the deformation of fixture and crossbeam. These additional deformations also increase with the increase in applied loading. This is visible in Fig. 5 where the discrepancy between the calculated deformation and crosshead displacement is larger for higher applied stresses. It is also illustrated that for determining specimen compliance, the elongation of the specimen should be measured with an extensometer on the specimen, rather than measuring crosshead displacement.

4.2. FWCF formulation for GLARE

Based on the previous discussion, it is reasonable to argue that the FWCF for GLARE specimens can be described by the ratio of compliances for the constant amplitude loading as described with Eq. (7). Fig. 6 shows these compliance ratios against $2a/W$ for GLARE 2A, GLARE 3 and GLARE 4B, which are also compared with work ratios calculated using the force and crosshead displacement, and the Dixon and Feddersen FWCF. Where the work ratio curves exhibit quite some differences in the shape of curves and the magnitude, it can be seen that the compliance ratios based on the equivalent delamination area have very similar trends for the GLARE with different grades. These compliance ratios for GLARE are all signifincntly lower than the Dixon and Feddersen FWCF, as explained in our previous paper [20]. In addition, the discrepancy between the standard FWCFs and the compliance curves increases greatly with the increase of crack length. Although the FWCF are substantially lower than the standard FWCFs, they cannot be neglected when implementing linear elastic mechanics to calculate the SIF.

To aid in the prediction of fatigue crack growth in GLARE, it is required that the FWCF can be described with an explicit formulation. For GLARE under constant amplitude fatigue loading, the change in applied work is determined by the increase in crack length and the delamination area. As formulated in Eq. (8), the FWCF can be divided into two parts. By using the equivalent delamination area, the compliance of GLARE is expressed as function of the delamination area. The delamination area is also associated with the crack length [26]. The final formulation of FWCF for GLARE therefore can be written as the function of $2a/W$. At a certain crack length a, there is a corresponding delamination area A. Fig. 7(a) presents the delamination correction F_f as function of $A/A_{\max}$, in which the contribution from the crack growth is removed. The delamination correction F_f decreases with the increase of $A/A_{\max}$. The relationship between $A/A_{\max}$ and $2a/W$ is shown in Fig. 7(b). Combining Fig. 7(a) and Fig. 7(b), the resulting delamination correction F_f against $2a/W$ for different grades of GLARE are provided in Fig. 8 and the corresponding polynomial fitting fuctions are also presented. It can be observed from Fig. 8 that the data for all specimens of a single GLARE grade together, despite some variability, can be fitted fairly well by one similar polynomial function. This means that the FWCF for GLARE can be formulated explicitly as

$$F(a) = \frac{1}{\sqrt{1-\left(\frac{2a}{W}\right)^2}}\left(1 + C_1\left(\frac{2a}{W}\right) + C_2\left(\frac{2a}{W}\right)^2 + C_3\left(\frac{2a}{W}\right)^3\right) \tag{9}$$

Here, the three formulations are distinct due to effective stiffness associated with the fibre lay-up. Thus, C_1, C_2 and C_3 can be related with the average Young's modulus of the fibre lay-up E_f between metal layers. Using polynomial fitting, C_1, C_2 and C_3 can be expressed as

$$C_1 = -7.67494 \times 10^{-6}E_f^3 + 6.02099 \times 10^{-4}E_f^2 - 0.011861E_f \tag{10}$$

$$C_2 = 2.3917 \times 10^{-5}E_f^3 - 1.9907 \times 10^{-3}E_f^2 + 0.0409723E_f \tag{11}$$

$$C_3 = -5.11225 \times 10^{-5}E_f^3 + 4.41151 \times 10^{-3}E_f^2 - 0.106717E_f \tag{12}$$

$$F(a) = (E_{FML}/E_f)\cdot(t_{FML}/t_f)^2 \tag{13}$$

In Fig. 9, the explicit forms of FWCF for GLARE are compared with the compliance ratios of all GLARE specimens, and with the Dixon and Feddersen FWCFs. This figure demonstrates that the explicit form of the FWCF for GLARE correlates well with all compliances ratio curves. The steep increase beyond 2a/W ~ 0.8 is attributed to the polynomial fit of equation (9) to the data beyond 2a/W = 0.8 (see Fig. 8), while multiplying with the Dixon (or any other) FWCF can increase to infinite at 2a/W = 1. As metioned in [20], the FWCF for GLARE increase slower with crack length, not up to infinite, but to a finite value as provided in

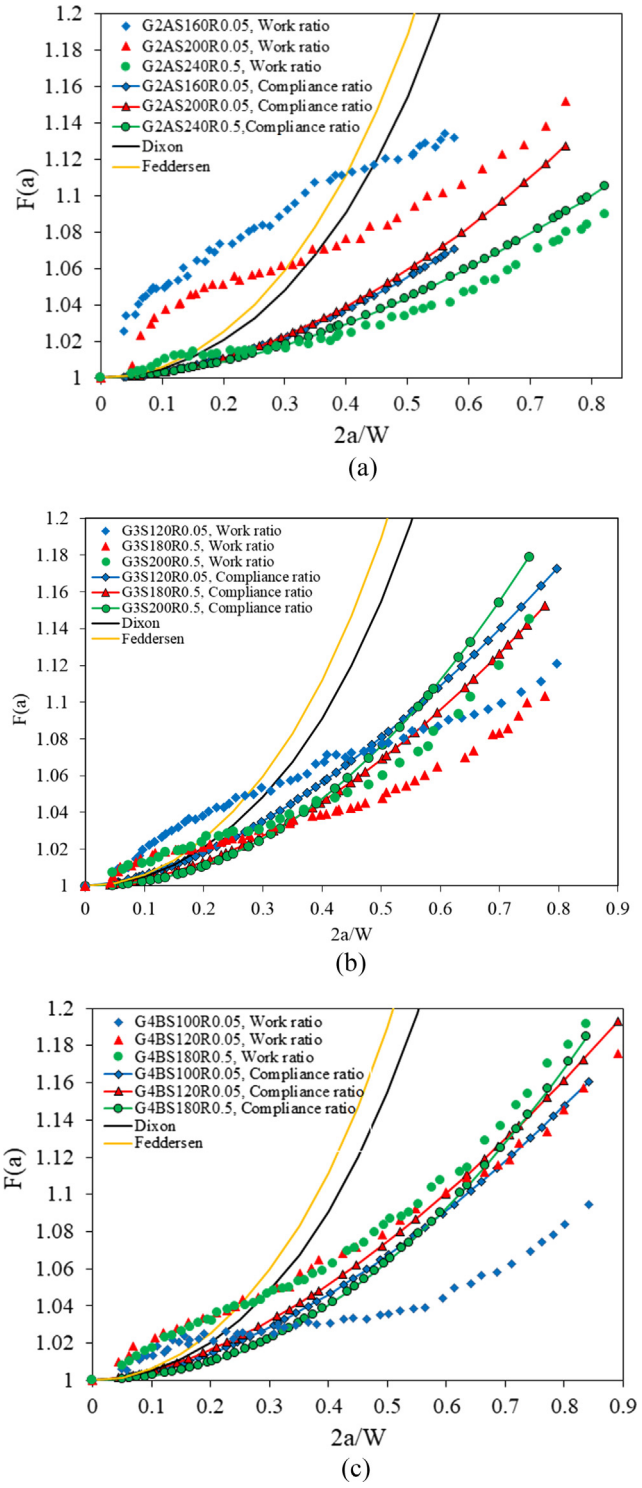

Fig. 6. Comparing FWCF for GLARE obtained by work ratio and compliance ratio, (a) GLARE 2A, (b) GLARE 3, and (c) GLARE 4B.

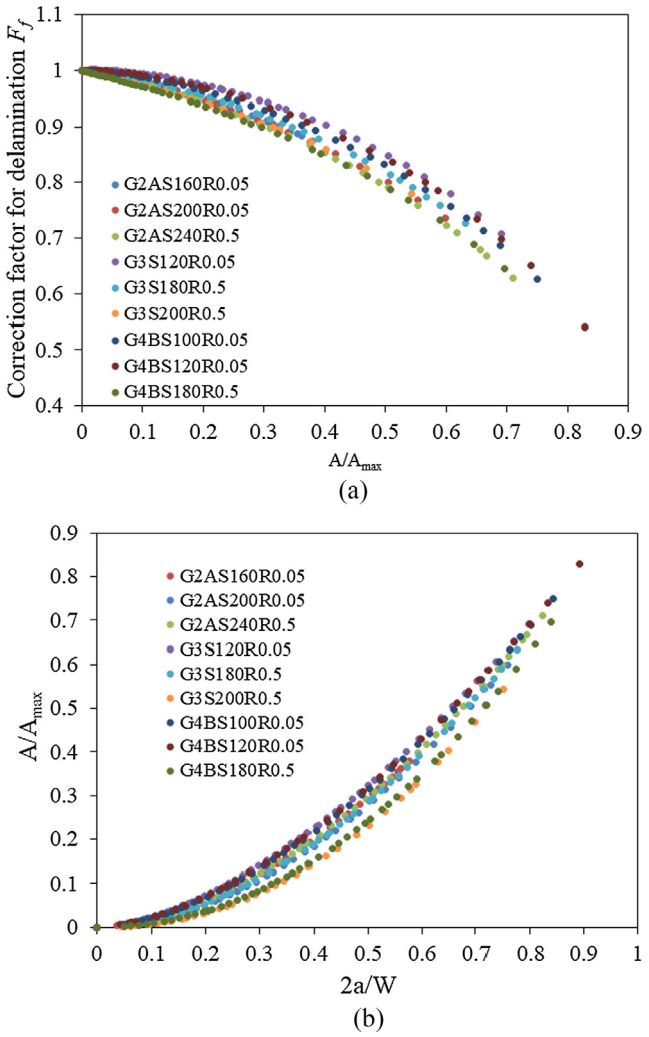

Fig. 7. Delamination correction for GLARE, (a) correction factor from delamination contribution, (b) delamination area vs. 2a/W.

Eq. (13). Hence, Eq. (9) has a limit of validity bounded by 2a/W < 0.8. This validity range is deemed to be sufficient for large scale structures. To accommodate accuracy in laboratory specimens with limited dimensions, it is proposed to use a linear relation from the value of Eq. (9) at 2a/W = 0.8 and the value of Eq. (13) at 2a/W = 1. The current hypothesis is that this FWCF of Eq. (9) applies to any FML with 0/0, 0/90, or 0/90/0 fibre orientations in-between the metal layers and similar delamination characteristics. Fatigue crack growth tests on FMLs with other metal and fibre polymer constituents are needed to validate this hypothesis.

5. Conclusion

The delamination areas in GLARE specimens made of different grades under fatigue loading were determined using strain field field measurements based on DIC. Subsequently, the elongations of GLARE under fatigue loading were calculated using the equivalent delamination areas, assuming it is equal to the measured delamination shapes. The calculated displacement of GLARE specimen itself is lower than that recorded by crosshead displacement, while they follow a rather similar trend. The calculated compliance ratio is proven to be suitable to establish the FWCF, which exhibits substantially less scatter than the method based on the crosshead displacement. It is concluded that combining the finite width correction for crack growth and the proposed delamination correction, allows for establishment of an explicit

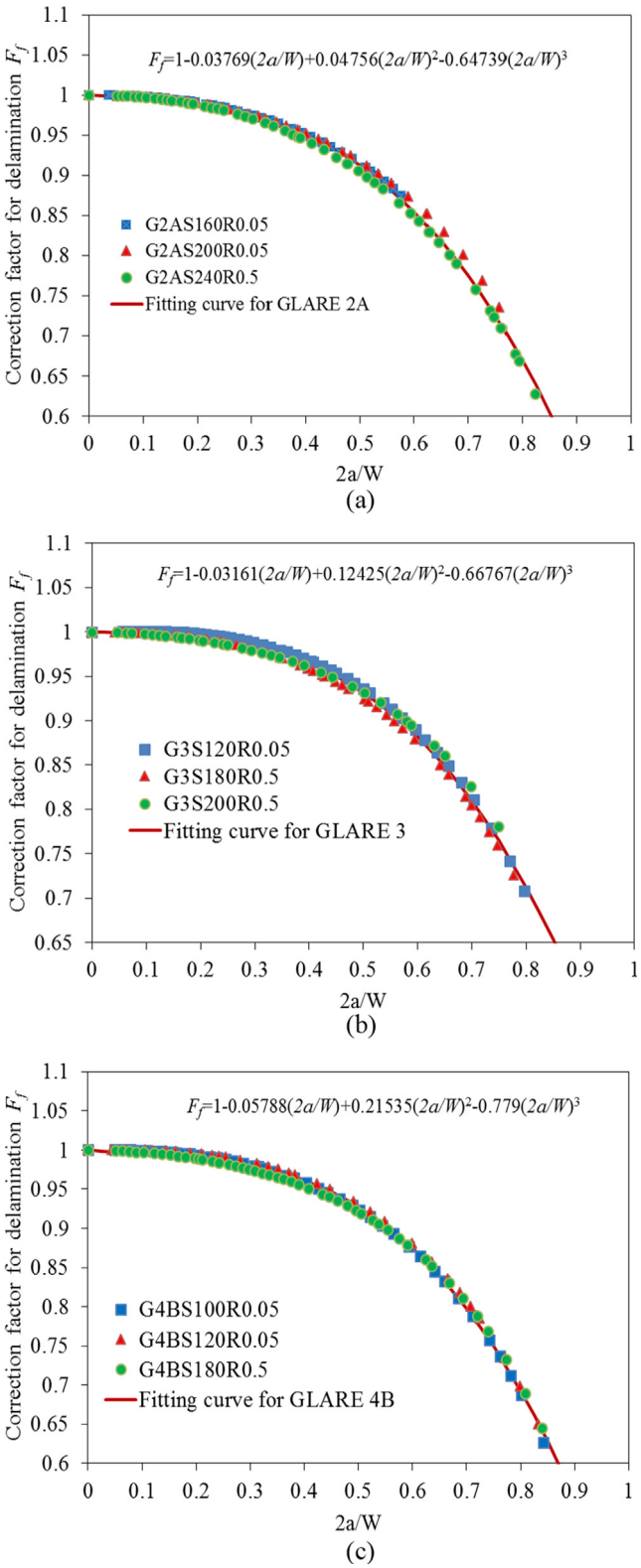

Fig. 8. Fitting correction formulation, (a) GLARE 2A, (b) GLARE 3, (c) GLARE 4B.

formulation of the FWCF for all GLARE grades. These explicit FWCFs aid the description and prediction of fatigue crack growth in GLARE using linear elastic mechanics.

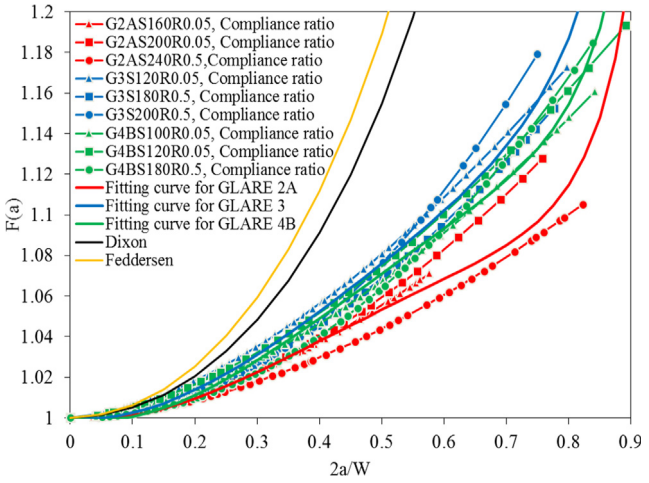

Fig. 9. Comparing explicit FWCF and compliance ratio curves.

Acknowledgements

This work is supported by the State Scholarship Fund from the China Scholarship Council (CSC), National Natural Science Foundation of China (Grant Nos. 11672089, 11572101), the Fundamental Research Funds for the Central Universities (Grant No. HIT.NSRIF.2017017) and Natural Science Foundation of Heilongjiang Province, China (Grant No. A2017003).

References

[1] Alderliesten RC. Fatigue and Fracture of Fibre Metal Laminates. Switzerland: Springer International Publishing AG; 2017.
[2] Paris PC, Gomez MP, Anderson WE. A rational analytic theory of fatigue. Trends Eng 1961;13:9–14.
[3] Alderliesten RC. The explanation of stress ratio effect and crack opening corrections for fatigue crack growth in metallic materials. Adv. Mater. Res. 2014;891–892:289–94.
[4] Alderliesten RC. How proper similitude principles could have improved our understanding about fatigue damage growth. Proceedings of the 28th ICAF Symposium – Helsinki, 3–5 June. 2015.
[5] Alderliesten RC. How proper similitude could improve our understanding of crack closure and plasticity in fatigue. Int J Fatigue 2016;82:263–73.
[6] Wilson GS. Fatigue crack growth prediction for generalized fiber metal laminates and hybrid materials. Delft: Delft University of Technology; 2013. PhD thesis.
[7] Westergaard HM. Bearing pressures through a slightly waved surface or through a nearly flat part of a cylinder, and related problems of cracks. J Appl Mech 1939;61:49–53.
[8] Koiter WT. An infinite row of collinear cracks in an infinite elastic sheet. Ingenieur-Archiv 1959;28(1):168–72.
[9] Irwin GR. Analysis of stresses and strains near the end of a crack traversing a plate. J Appl Mech 1957;24:361–4.
[10] M. Isida. Crack tip stress intensity factors for the tension of an eccentrically cracked strip. Lehigh University, Department of Mechanics Report, 1965.
[11] Brown Jr WF, Srawley JE. Plane strain crack toughness testing of high strength metallic materials. ASTM STP No. 410, American Society of Testing and Materials. 1969.
[12] Forman RG, Kobayashi AS. On the axial rigidity of a perforated strip and the strain energy release rate in a centrally notched strip subjected to uniaxial tension. J Basic Eng 1964:693–7.
[13] Tada H. A note on the finite width corrections to the stress intensity factor. Eng Fract Mech 1971;3:345–7.
[14] Feddersen C. Discussion to: plane strain crack toughness testing. American Society of Testing and Mater 1967:410.
[15] Dixon JR. Stress distribution around a central crack in a plate loaded in tension: effect of finite width of plate. J. Royal Aeronaut. Soc. 1960;64:141–5.
[16] Bowie OL, Neal DM. A note on the central crack in a uniformly stressed strip. Eng Fract Mech 1970;2:181–2.
[17] Irwin GR. Fracture testing of high-strength sheet materials under conditions appropriate for stress analysis. NRL Report 5486 1960.
[18] Liebowitz H, Eftis J. Correcting for nonlinear effects in fracture toughness testing. Nucl Eng Des 1972;18(3):457–67.
[19] Ravi KS. Chandran. Insight on physical meaning of finite-width-correction factors in stress intensity factor (K) solutions of fracture mechanics. Eng Fract Mech 2017;186:399–409.
[20] Zhao Y, Alderliesten R, Zhou ZG, Fang GD, Zhang JZ, Benedictus R. On the physics of applying finite width and geometry correction factors in fatigue crack growth predictions of GLARE. Int J Fatigue 2018;117:189–95.
[21] Alderliesten RC, Schijve J, van der Zwaag S. Application of the energy release rate approach for delamination growth in Glare. Eng Fract Mech 2006;73:697–709.
[22] ASTM E647-15e1. Standard Test Method for Measurement of Fatigue Crack Growth Rates. American Society for Materials and Testing, ASTM International, 2015. West Conshohocken, USA: 1-49. doi: 10.1520/E0647-15E01.
[23] Khan S. Fatigue crack & delamination growth in fibre metal laminates under variable amplitude loading. Delft: Delft University of Technology; 2013. Ph.D. thesis.
[24] Rodi R. The residual strength failure sequence in fibre metal laminates. Delft: Delft University of Technology; 2012. Ph.D. thesis.
[25] Huang Y, Liu JZ, Huang X, Zhang JZ, Yue GQ. Delamination and fatigue crack growth behaviour in Fiber Metal Laminates (Glare) under single overloads. Int J Fatigue 2015;78:53–60.
[26] Alderliesten RC. Analytical prediction model for fatigue crack propagation and delamination growth in Glare. Int J Fatigue 2007;29:628–46.
[27] Takamatsu T, Matsumura T, Ogura N, Shimokawa T, Kakuta Y. Fatigue crack growth properties of a GLARE3-5/4 fiber/metal laminate. Eng Fract Mech 1999;63:253–72.